Reconstruction of a Motion and Attenuation Corrected Activity Distribution in Gated TOF-PET

Ahmadreza Rezaei[1], Michel Defrise[2], Johan Nuyts[1]

***Abstract*—In this work, we demonstrate a framework in which the gated TOF-PET emission data are used to reconstruct a single activity image (which is corrected for attenuation), together with motion parameters that deform the activity reconstruction (of the reference frame) to each of the frames. We compare the reconstructions to independent and registered (post-reconstruction) MLACF reconstructions of each frame. We propose a joint estimation method that avoids selecting a reference frame and provides low bias and variance compared to methods that select a reference frame from among the gated frames. Reconstruction results are also shown for the 3D breathing XCAT phantom.**

I. Introduction

Various methods have been proposed that deal with gated PET emission data. Commonly the gated PET data are reconstructed independently (in each frame) and are registered (post-reconstruction) and then averaged to obtain a motion-free activity image [1]. More recently, methods have been proposed that take advantage of the emission data from all gates and combine the two reconstruction and registration steps [2]. In the latter approach, the method estimates one activity image together with multiple transformation parameters that deform the reconstructed activity image (in the reference frame) to the desired gates. Although promising results were reported, more studies are warranted on the topic, e.g. to investigate the selection of the reference frame and its effect on the final activity image and motion parameter estimates.

Furthermore, attenuation correction in gated PET studies has always been a challenge, and is at times avoided. Since the TOF-PET data determine the attenuation factors sinogram up to a scale [3], the availability of time-of-flight (TOF) PET data provides a means to overcome this longstanding problem. In this contribution we use the newly developed algorithm MLACF [4], [5], which estimates an activity image and a sinogram of the attenuation factors from the gated TOF-PET emission data.

II. Methods

The proposed method jointly estimates an activity image together with transformation parameters that deform the activity image to a corresponding frame of the gated TOF-PET data. By using a modified version (for gated TOF-PET data) of the MLACF algorithm, we obtain an activity image which is corrected for attenuation, and with a similar approach to that in [6] we estimate the transformation parameters of either a rigid or non-rigid motion model, which deforms the activity of the reference frame to each of the gates. The activity and motion estimates are then updated sequentially. In this framework, the activity image can be reconstructed in either a virtual reference frame (VRF) or a specific reference frame (SRF), depicted in figure 1. In both cases the activity image and the motion parameters are initialized by a uniform disk of activity and the identity motion parameter for each frame, respectively. With a non-rigid motion model, the computation of a displacement field, and the use of its transpose (replaced by the inverse due to numerical issues) are required to deform the activity reconstruction of the reference frame to each of the frames and back. Details will be provided at the conference.

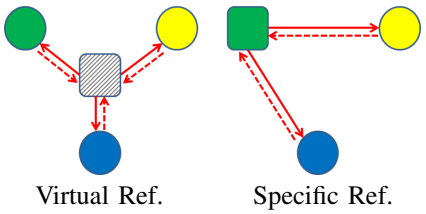

Fig. 1. Depiction of the joint estimation framework where the single activity reconstruction is obtained in a virtual (left) or a specific (right) reference frame relative to the gated PET data. The colored circles and squares depict 3 different frames. The squares represent the frame that the activity reconstruction will be reconstructed in, the solid arrows are the displacements that are to be estimated, and the dotted arrows are the inverse displacements that are computed from their corresponding displacement estimates.

Since there are no constraints on the reference frame in the VRF case, it is likely that the activity image is reconstructed at a displacement equal to the mean of the frame positions (which we call the 'average position frame'). In contrast, a feature of the SRF case is that it requires one less displacement and its inverse to be estimated. In the following, we investigate the reconstruction results of the joint activity and motion estimation method and compare the results to independent and registered MLACF reconstructions of each frame. We then briefly look into the effects of the choice of the reference frame on the estimated activity reconstructions.

III. Simulation Design

The simulation specifications were adjusted according to the Siemens Biograph mCT scanner specifications. In the 2D simulations, the TOF-PET emission data consist of 200 radial bins of 0.4 cm width, 168 projection angles over 180 deg, and 13 TOF-bins of 312 ps width with an effective TOF resolution of 580 ps. An oversampling of 3 was also used during simulations to account for a slight mismatch (between

This research is supported by a research grant (GOA) from K.U.Leuven, FWO project G027514N and by Siemens Healthcare, Anderlecht, Belgium.
[1]Nuclear Medicine, K.U.Leuven, B-3000 Leuven, Belgium. [2]Nuclear Medicine Department, Vrije Universiteit Brussel, B-1090 Brussels, Belgium.

projector and simulations), and the reconstructed image had 200 $\times$ 200 pixels of 0.4 cm width. In the 3D simulation, the TOF-PET data are organized as 5D sinograms, consisting of 200 radial bins, 168 azimuthal angles, 9 co-polar angles, 109 planes, and 13 TOF-bins. The reconstructed image had a 200 $\times$ 200 $\times$ 109 volume grid with a voxel width of 0.4 cm and 0.2 cm in the transaxial and axial directions, respectively.

A. 2D Thorax Phantom

Figure 2 shows the 2D activity and attenuation images of 3 simulated frames. An increase in the size of the lungs and a displacement of the tumor lesion were used to simulate non-rigid deformations between the 3 frames. TOF-PET emission data were obtained for each frame assuming a scan duration ratio of 0.31, 0.46 and 0.23 for each frame, respectively.

1) Reconstructions: After adding Poisson noise to the emission data, a single activity image was reconstructed together with 3 sinograms of the attenuation factors in each frame and 3/2 displacement estimates for the VRF/SRF joint estimation cases. We assumed that the total amount of activity in all frames was available, and the MLACF scale problem [3] was solved accordingly. The results are then compared to independent and registered MLACF activity reconstructions of each frame. The post-reconstruction registration algorithm was the same as the one used in joint activity and motion estimation framework. The Demons' [7], [8] registration algorithm was used in two resolution levels in each iteration, and the displacements were computed using a symmetric Demons' update rule. This was to take full advantage of the independent reconstructions of each frame. The independent MLACF reconstructions are obtained after 5 iterations of 24 subsets, and the joint reconstructions are after 10 iterations of 24 subsets where the first iteration assumes a rigid motion model.

2) Noise Realization: The effect of the reference frame selection on bias and variance values of the reconstructed activity image (when deformed to each frame) is analyzed for 100 different noise realizations. Bias in each frame is computed as the average absolute pixel by pixel difference between the average of the true activity images and the joint activity reconstructions deformed to each of the frames. The results are reported together with the results of independent and registered MLACF reconstruction of each frame.

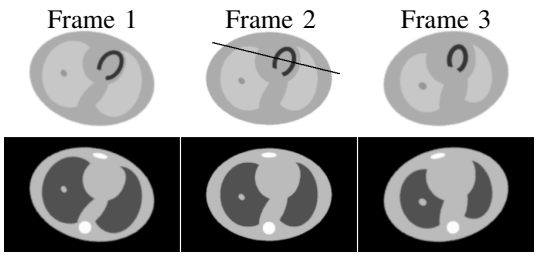

Fig. 2. Activity (top) and attenuation (bottom) images of the 2D thorax phantom deformed into 3 frames.

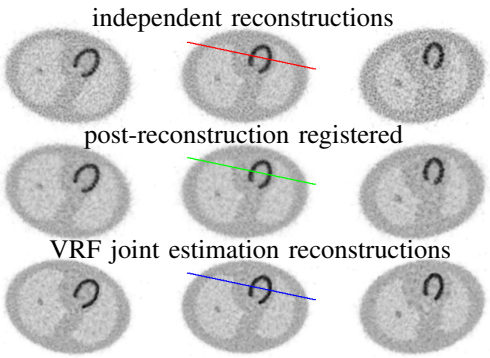

Fig. 3. Independent MLACF activity reconstructions (top), registered activity reconstructions of each frame post-reconstruction (center), and the deformed activity reconstruction of the VRF joint estimation method (bottom).

B. 3D Breathing XCAT Phantom

The XCAT phantom was used to generate realistic respiratory motion. A maximum diaphragm motion of 2.0 cm and a maximum anterior-posterior motion of 1.2 cm was used to simulate the breathing cycle, which was gated into 8 (motion-free) frames of 1.25 min durations each. After adding Poisson noise to the emission measurements, a single activity image was reconstructed in a virtual reference frame, together with a set of 8 attenuation factor sinograms and 8 displacement fields. The joint reconstructions are obtained after 6 iterations of 24 subsets, assuming a rigid motion model for the first iteration and a non-rigid motion model for the following 5 iterations. The independent MLACF reconstruction of the frames are after 3 iterations of 24 subsets and the registered activity images are obtained after the same updates of the Demons' registration algorithm.

IV. Results

A. 2D Thorax Phantom

1) Reconstructions: Figure 3 shows independent MLACF and post-reconstruction registered activity reconstructions of each frame together with the VRF joint reconstruction after the single activity image was deformed to each frame. Since the scan duration of each frame was different, the independent activity reconstructions have a different noise response. The registered activity images of each frame (post-reconstruction) show a similar noise response between frames, however compared to the joint estimation reconstructions, the registered reconstructions suffer from a degraded resolution.

2) Noise Realization: Table I reports bias and variance of the independent MLACF activity reconstructions of each frame together with the post-reconstruction registered activity images (MLACF-PRR), and the VRF/SRF joint estimation activity reconstruction (SRF-i, $i = 1, 2, 3$, where i determines the reference frame), after the activity reconstruction is deformed to each frame. Table I shows that the selection of the reference frame influences bias and variance in the reconstructions. Moreover, it shows that the VRF case achieves low bias and variance, and that the largest error occurs when the motion parameters need to explain larger displacements (SRF-1 and SRF-3).

TABLE I
BIAS AND VARIANCE OF THE INDEPENDENT MLACF, POST-RECONSTRUCTION REGISTERED, AND THE VRF/SRF JOINT ESTIMATED ACTIVITY IMAGES OF EACH FRAME

	Frame 1	Frame 2	Frame 3
MLACF	0.189 (1.539)	0.195 (1.061)	0.220 (2.296)
MLACF-PRR	0.180 (0.689)	0.204 (0.634)	0.218 (0.784)
VRF	0.167 (0.589)	0.191 (0.575)	0.191 (0.627)
SRF-1	0.168 (0.910)	0.193 (0.681)	0.183 (0.732)
SRF-2	0.180 (0.738)	0.193 (1.001)	0.176 (0.784)
SRF-3	0.183 (0.627)	0.203 (0.623)	0.265 (0.838)

B. 3D Breathing XCAT Phantom

Figure 4 shows the true activity image of frame 5 together with the independent activity reconstruction of the frame (MLACF), the post-reconstruction registered image of the frame (MLACF-PRR), and the activity reconstruction of the VRF joint estimation method (VRF-JE). It is interesting to see that the activity reconstruction of the joint estimation provides a more accurate reconstruction compared to the post-reconstruction registered activity image.

V. CONCLUSION

This work investigates the effect of the choice of the reference frame in joint activity and motion estimation methods, and its influence on the final activity reconstruction. The newly proposed MLACF algorithm is modified to account for gated TOF-PET emission data and is used for the estimation of attenuation corrected activity images. The noise simulation suggests that when the reference frame is chosen close to the 'average position frame', reconstructions have the smallest error. The 2D/3D simulations show a qualitative improvement in the activity reconstructions compared to post-reconstruction registered activity images.

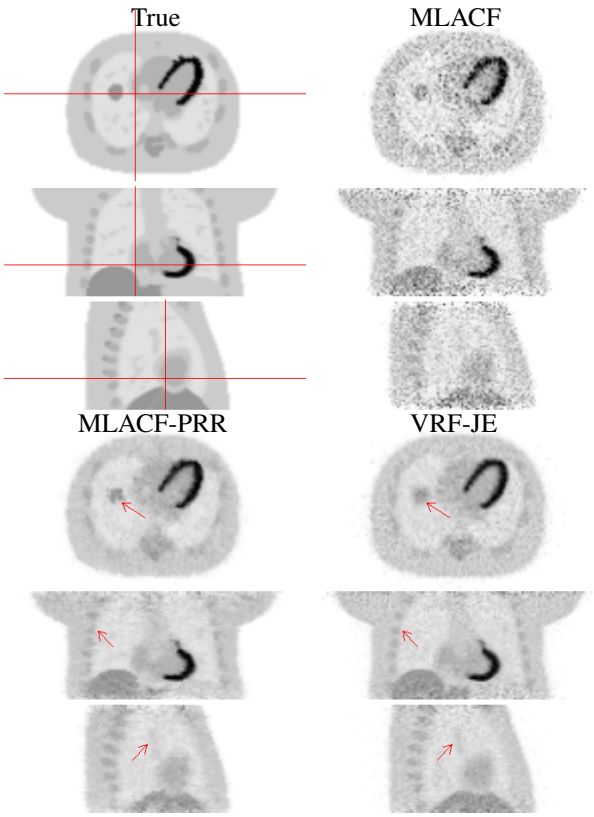

Fig. 4. The true activity image of frame 5 (top-left) and its independent MLACF activity reconstruction (top-right) shown together with the post-reconstruction registered activity (bottom-left) and the deformed activity reconstruction of the VRF joint estimation method (bottom-right).

REFERENCES

[1] M. Dawood, F. Buther, X. Jiang, and K. P. Schafers, "Respiratory motion correction in 3-D PET data with advanced optical flow algorithms." *IEEE Trans. Med. Imaging*, vol. 27, no. 8, pp. 1164–75, Aug. 2008.

[2] M. Blume, A. Martinez-Möller, A. Keil, N. Navab, and M. Rafecas, "Joint reconstruction of image and motion in gated positron emission tomography." *IEEE Trans. Med. Imaging*, vol. 29, no. 11, pp. 1892–906, Nov. 2010.

[3] M. Defrise, A. Rezaei, and J. Nuyts, "Time-of-flight PET data determine the attenuation sinogram up to a constant." *Phys. Med. Biol.*, vol. 57, no. 4, pp. 885–99, Feb. 2012.

[4] ——, "Transmission-less attenuation correction in time-of-flight PET: analysis of a discrete iterative algorithm." *Phys. Med. Biol.*, vol. 59, no. 4, pp. 1073–95, Feb. 2014.

[5] A. Rezaei, M. Defrise, and J. Nuyts, "ML-reconstruction for TOF-PET with simultaneous estimation of the attenuation factors." *IEEE Trans. Med. Imaging*, vol. 33, no. 7, pp. 1563–72, Jul. 2014.

[6] A. Rezaei and J. Nuyts, "Simultaneous reconstruction of the activity image and registration of the CT image in TOF-PET," in *2013 IEEE Nucl. Sci. Symp. Med. Imaging Conf. Rec.* IEEE, Oct. 2013, pp. 1–3.

[7] J. P. Thirion, "Image matching as a diffusion process: an analogy with Maxwell's demons," *Med. Image Anal.*, vol. 2, no. 3, pp. 243–260, Sep. 1998.

[8] T. Vercauteren, X. Pennec, A. Perchant, and N. Ayache, "Diffeomorphic demons: efficient non-parametric image registration." *Neuroimage*, vol. 45, no. 1 Suppl, pp. S61–72, Mar. 2009.